Regular Article

blood



HEMATOPOIESIS AND STEM CELLS

# Setdb1 maintains hematopoietic stem and progenitor cells by restricting the ectopic activation of nonhematopoietic genes

Shuhei Koide,[1] Motohiko Oshima,[1] Keiyo Takubo,[2] Satoshi Yamazaki,[3] Eriko Nitta,[1] Atsunori Saraya,[1] Kazumasa Aoyama,[1] Yuko Kato,[1] Satoru Miyagi,[1] Yaeko Nakajima-Takagi,[1] Tetsuhiro Chiba,[4] Hirotaka Matsui,[5] Fumio Arai,[6] Yutaka Suzuki,[7] Hiroshi Kimura,[8] Hiromitsu Nakauchi,[3,9] Toshio Suda,[10,11] Yoichi Shinkai,[12] and Atsushi Iwama[1]

[1]Department of Cellular and Molecular Medicine, Graduate School of Medicine, Chiba University, Chiba, Japan; [2]Department of Stem Cell Biology, Research Institute, National Center for Global Health and Medicine, Tokyo, Japan; [3]Division of Stem Cell Therapy, Center for Stem Cell Biology and Regenerative Medicine, Institute of Medical Science, University of Tokyo, Tokyo, Japan; [4]Department of Medicine and Clinical Oncology, Graduate School of Medicine, Chiba University, Chiba, Japan; [5]Department of Molecular Laboratory Medicine, Faculty of Life Sciences, Kumamoto University, Kumamoto, Japan; [6]Department of Stem Cell Biology and Medicine, Graduate School of Medical Sciences, Kyushu University, Fukuoka, Japan; [7]Laboratory of Functional Genomics, Department of Medical Genome Sciences, Graduate School of Frontier Sciences, University of Tokyo, Tokyo, Japan; [8]Department of Biological Sciences, Graduate School of Bioscience and Biotechnology, Tokyo Institute of Technology, Yokohama, Japan; [9]Institute for Stem Cell Biology and Regenerative Medicine, Stanford University School of Medicine, Stanford, CA; [10]Cancer Science Institute, National University of Singapore, Singapore, Singapore; [11]International Research Center for Medical Sciences, Kumamoto University, Kumamoto City, Japan; and [12]Cellular Memory Laboratory, RIKEN, Wako, Japan

## Key Points

- Setdb1, an H3K9 histone methyltransferase, is essential for the maintenance of HSPCs.
- Setdb1 restricts the activation of nonhematopoietic genes, such as gluconeogenic pathway genes, to maintain HSPCs.

**Setdb1, also known as Eset, is a methyltransferase that catalyzes trimethylation of H3K9 (H3K9me3) and plays an essential role in the silencing of endogenous retroviral elements (ERVs) in the developing embryo and embryonic stem cells (ESCs). Its role in somatic stem cells, however, remains unclear because of the early death of *Setdb1*-deficient embryos. We demonstrate here that Setdb1 is the first H3K9 methyltransferase shown to be essential for the maintenance of hematopoietic stem and progenitor cells (HSPCs) in mice. The deletion of *Setdb1* caused the rapid depletion of hematopoietic stem and progenitor cells (HSPCs), as well as leukemic stem cells. In contrast to ESCs, ERVs were largely repressed in *Setdb1*-deficient HSPCs. A list of nonhematopoietic genes was instead ectopically activated in HSPCs after reductions in H3K9me3 levels, including key gluconeogenic enzyme genes fructose-1,6-bisphosphatase 1 (*Fbp1*) and *Fbp2*. The ectopic activation of gluconeogenic enzymes antagonized glycolysis and impaired ATP production, resulting in a compromised repopulating capacity of HSPCs. Our results demonstrate that Setdb1 maintains HSPCs by restricting the ectopic activation of nonhematopoietic genes detrimental to their function and uncover that the gluconeogenic pathway is one of the critical targets of Setdb1 in HSPCs. (*Blood*. 2016;128(5):638-649)**

## Introduction

In mammals, DNA methylation and trimethylation at histone H3 lysine 9 (H3K9me3) are strongly associated with each other and cooperatively silence genes and retroelements.[1] Although DNA methylation is considered to repress the expression of viral genes in differentiated cells, repression in pluripotent cells is mediated by DNA methylation and histone modifications.[2] There are 5 members of the SUV39 family that catalyze H3K9 methylation: Suv39h1, Suv39h2, G9a, GLP, and Setdb1. Setdb1 (also known as Eset) is an H3K9 trimethyltransferase that is mainly localized in euchromatic regions. Homozygous mutations of *Setdb1* have been shown to result in peri-implantation lethality between 3.5 and 5.5 dpc.[3] Setdb1 represses subfamilies of endogenous retroviruses (ERVs) in a DNA methylation-independent manner in murine embryonic stem cells (ESCs) and the early embryo.[2,4,5] Kap1 (also known as Trim28 and Tif1β), a scaffold protein targeted to specific sequences through KRAB zinc finger proteins, recruits Setdb1. Thus, Kap1 and Setdb1 cooperatively repress ERVs via the enrichment of H3K9me3 in ESCs.[2,6] However, their role in adult somatic stem cells remained largely obscure.

It has been reported that the amount of euchromatin decreases while the layer of heterochromatin at the nuclear envelop increases during the differentiation of hematopoietic stem cells (HSCs). Prevention of heterochromatin formation by pharmacological inhibition of G9a, which catalyzes H3K9me2, results in delayed HSC differentiation. Thus, the proper transition from euchromatin to heterochromatin mediated by H3K9 methylation is required for efficient HSC differentiation.[7] Of interest, however, is that G9a is dispensable for the maintenance of HSCs.[8] We previously characterized the hematopoietic cell-specific deletion of *Kap1* in mice and reported that Kap1

Submitted January 21, 2016; accepted May 31, 2016. Prepublished online as *Blood* First Edition paper, June 14, 2016; DOI 10.1182/blood-2016-01-694810.

The online version of this article contains a data supplement.

The publication costs of this article were defrayed in part by page charge payment. Therefore, and solely to indicate this fact, this article is hereby marked "advertisement" in accordance with 18 USC section 1734.

is essential for the maintenance of HSCs. In collaboration with heterochromatin protein 1 (HP1) proteins, Kap1 functions as a critical repressive machinery that targets genes not normally activated in the hematopoietic compartment, thereby maintaining the transcriptional signature specific to HSCs.[9] These findings suggested the H3K9me3-mediated regulation of HSC functions and a role for Setdb1 in this process.

In the present study, we examined mice in which *Setdb1* was deleted specifically in hematopoietic cells and found that Setdb1 is the first H3K9 methyltransferase shown to be essential for the maintenance of hematopoietic stem and progenitor cells (HSPCs). Comprehensive transcriptome and epigenomic analyses revealed that Setdb1 is mostly dispensable for the silencing of ERVs in HSPCs, but preferentially targets nonhematopoietic genes, the ectopic expression of which compromises the function of HSPCs. Among nonhematopoietic target genes, we demonstrate that the gluconeogenic pathway is one of the critical targets of Setdb1 in HSPCs.

## Materials and methods

### Metabolite extraction and metabolome analysis

Cells were washed twice by 5% mannitol solution (10 mL first and then 2 mL), treated with 800 μL of methanol, and left at rest for 30 seconds to inactivate enzymes. The cell extract was then treated with 550 μL Milli-Q water containing internal standards (H3304-1002; Human Metabolome Technologies [HMT]) and left at rest for another 30 seconds. The extract was obtained and centrifuged at 2300 × *g* and 4°C for 5 minutes, and then 800 μL upper aqueous layer was centrifugally filtered through a Millipore 5-kDa cutoff filter (UltrafreeMC-PLHCC; HMT) to remove macromolecules (9100 × *g*, 4°C, 120 min). The filtrate was centrifugally concentrated and resuspended in 50 μL Milli-Q water for metabolome analysis at HMT. Metabolome analysis was conducted by *C-SCOPE* package of HMT, using capillary electrophoresis time-of-flight mass spectrometry (CE-TOFMS) for cation analysis and CE-tandem mass spectrometry (CE-MS/MS) for anion analysis. Briefly, CE-TOFMS analysis was carried out using an Agilent CE capillary electrophoresis system equipped with an Agilent 6210 TOF mass spectrometer (Agilent Technologies). The spectrometer was scanned from *m/z* 50 to 1000.[10,11] Peaks were extracted using MasterHands automatic integration software[12] and MassHunter Quantitative Analysis B.04.00 (Agilent Technologies) to obtain peak information, including *m/z*, peak area, and migration time (MT). Signal peaks were annotated according to the HMT metabolite database on the basis of their *m/z* values with the MTs. Concentrations of metabolites were calculated by normalizing the peak area of each metabolite with respect to the area of the internal standard and by using standard curves with 3-point calibrations. Detected metabolites were plotted on metabolic pathway maps using VANTED software.[13]

### RNA-sequencing

Total RNA was subjected to reverse transcription and amplification for 16 cycles, respectively, with SMARTer Ultra Low Input RNA Kit for Sequencing v3 (Clontech). After sonication with an ultrasonicator (Covaris), the libraries for RNA-seq were generated from 50 ng fragmented DNA with 8 cycles of amplification, using a NEBNext Ultra DNA Library Prep Kit (New England BioLabs). After the libraries were quantified, using a high-sensitivity Chip on Bioanalyzer (Agilent), the samples were subjected to sequencing with a Hiseq1500 (Illumina), and 61 cycles of the sequencing reactions were performed. TopHat2 (version 2.0.13; with default parameters) and Bowtie2 (version 2.1.0) were used to align to the reference mouse genome (mm9 from University of California, Santa Cruz Genome Browser; http://genome.ucsc.edu/). Then gene expression values were calculated as reads per kilobase of exon unit per million mapped reads, using cufflinks (version 2.2.1). Total read number per ERV family was determined as described.[14] Proviruses with a Smith–Watterman score of at least 5000 (Repeatmasker) were used to properly annotate ERVs.

### ChIP-sequencing

Chromatin immunoprecipitation (ChIP) assays were performed as previously described.[15] Briefly, $1 \times 10^5$ pooled bone marrow (BM) $Lin^-$ $Sca\text{-}1^+$ $c\text{-}Kit^+$ (LSK) cells were subjected to immunoprecipitation, using anti-H3K27me3 (07449; Millipore) and anti-H3K9me3 (clone 2F3).[16] Sheep anti-rabbit immunoglobulin G (IgG) and sheep anti-mouse IgG Dynabeads were used to capture anti-H3K27me3 and anti-H3K9me3 ($IgG_1$), respectively. The RPM (reads per million mapped reads) values of the sequenced read were calculated every 2000-base pair bin with a shifting size of 200 base pairs, using bedtools. To evaluate the histone modification mark of each gene, the RPM values of the region from 4 kb upstream to 4 kb downstream of the transcription start site (TSS) of the immunoprecipitated samples were divided by RPM of corresponding input. To visualize with Integrative Genomics Viewer (http://www.broadinstitute.org/igv), the RPM values of the immunoprecipitated samples were normalized by subtracting the RPM values of the input samples in each bin and converted to a bigwig file, using the wigToBigWig tool.

### Reduced representation bisulfite sequencing

Five hundred nanograms DNA was digested by *Msp*I (Takara), and fragments cut into 150-250 bp were selectively extracted. Methylated adaptor-oligos (Illumina) were ligated to both ends of the fragments, followed by bisulfite conversion and polymerase chain reaction (PCR) amplification to prepare libraries for sequencing. The libraries were sequenced under single-end 50 bp protocol, using Hiseq1500 sequencer (Illumina). Differentially methylated nucleotides/regions were identified using methylKit.[17]

### Accession numbers

Data were deposited in DNA Data Bank of Japan (RNA-sequence, DRA004191; ChIP-sequence, DRA002605; reduced representation bisulfite sequencing [RRBS], DRA002147, DRA002148, DRA002149, DRA002150, DRA002151, DRA002152).

## Results

### Deletion of *Setdb1* leads to the rapid depletion of HSPCs and leukemic stem cells

To delineate the function of Setdb1 in HSPCs, we conditionally deleted *Setdb1* by crossing $Setdb1^{fl/fl}$ mice with *Rosa:Cre-ERT* (*Cre-ERT*) mice. We transplanted BM cells from *Cre-ERT* control and *Cre-ERT; *$Setdb1^{fl/fl}$ mice without competitor cells into lethally irradiated recipient mice. After confirming engraftment, we deleted *Setdb1* by intraperitoneal injection of tamoxifen at 4 weeks after transplantation. We hereafter refer to the recipient mice reconstituted with *Cre-ERT* and $Setdb1^{\Delta/\Delta}$ cells as wild-type (WT) and $Setdb1^{\Delta/\Delta}$ mice, respectively. The deletion of *Setdb1* was efficient, as judged by the genomic PCR and the reverse transcription (RT)-PCR of donor-derived BM progentor cells (Figure 1A-B). All $Setdb1^{\Delta/\Delta}$ mice died within 21 days of the initial injection of tamoxifen (Figure 1C) because of severe hematopoietic failure, as evident in BM sections (Figure 1D). Therefore, we subsequently examined hematopoiesis in $Setdb1^{\Delta/\Delta}$ mice 2 weeks after the initiation of the tamoxifen injection. Although the proportion of each hematopoietic lineage in the peripheral blood (PB) was not significantly changed in $Setdb1^{\Delta/\Delta}$ mice (Figure 1E), the numbers of BM cells and primitive hematopoietic cells, including $CD34^-Lin^-Sca\text{-}1^+c\text{-}Kit^+$ ($CD34^-$LSK) HSCs, $CD34^+$LSK multipotent progenitor cells, common myeloid progenitors, and granulocyte/macrophage progenitors (GMPs), but not megakaryocyte/erythrocyte progenitors

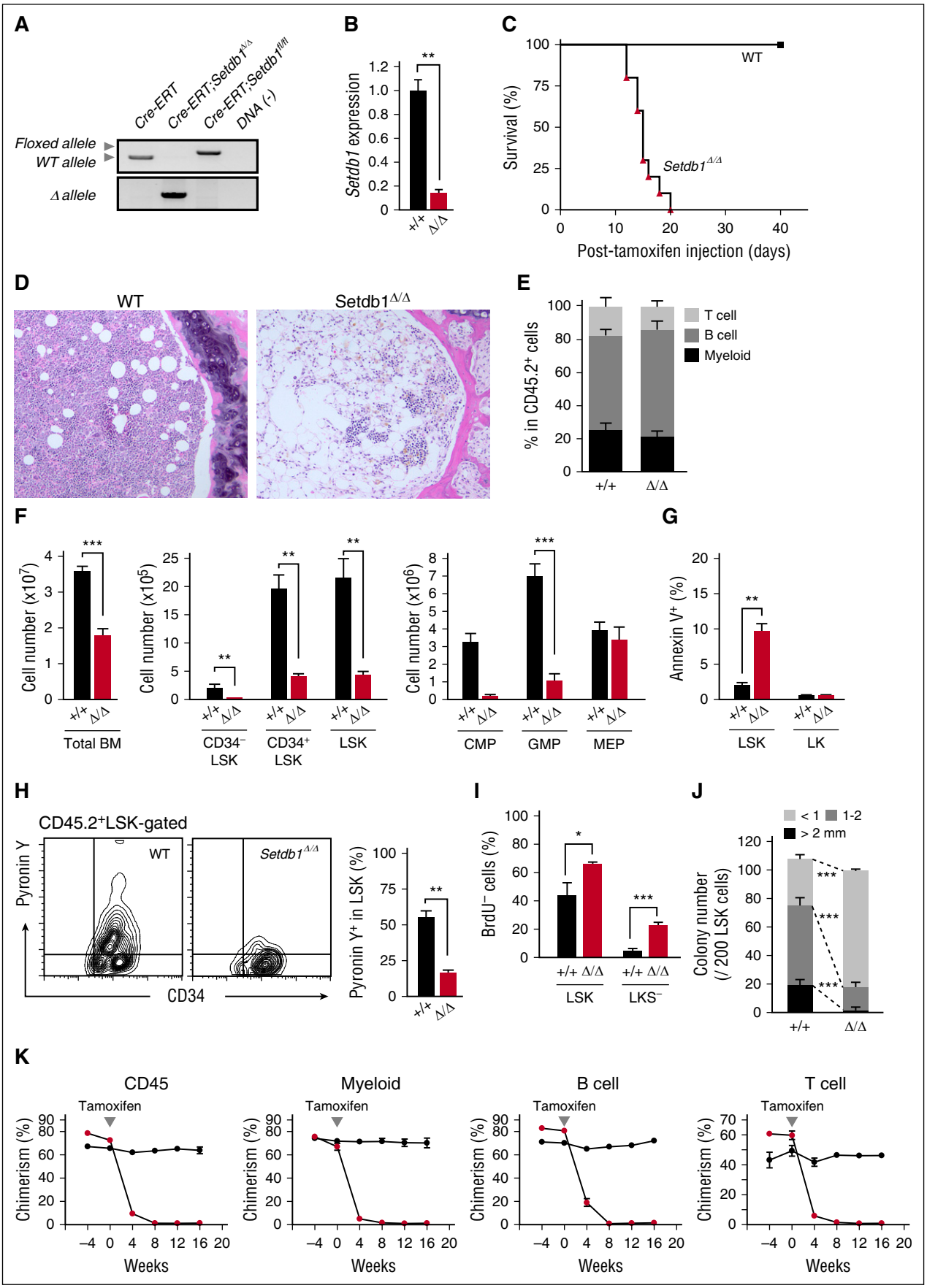


**Figure 1.**

were markedly lower in *Setdb1*$^{\Delta/\Delta}$ mice than in WT mice (Figure 1F). Apoptotic cell death was enhanced in *Setdb1*$^{\Delta/\Delta}$ LSK cells (Figure 1G), and mitochondrial reactive oxygen species levels were also increased in *Setdb1*$^{\Delta/\Delta}$ CD34$^-$LSK HSCs and CD34$^+$LSK multipotent progenitors (supplemental Figure 1, available on the *Blood* Web site). However, RNA content detected by Pyronin Y staining was significantly lower (Figure 1H), and the incorporation of BrdU was significantly less (Figure 1I), in *Setdb1*$^{\Delta/\Delta}$ LSK cells than in WT cells, suggesting impaired cell proliferation. Correspondingly, *Setdb1*$^{\Delta/\Delta}$ LSK cells gave rise to significantly smaller colonies than WT cells (Figure 1J). The heterozygous deletion of *Setdb1* also mildly compromised the proliferation of HSPCs. *Setdb1*$^{+/\Delta}$ LSK cells showed mildly impaired proliferation in culture with a significant reduction of LSK cells (supplemental Figure 2A-D). In addition, *Setdb1*$^{+/\Delta}$ LSK cells generated fewer colonies, although the reduction in colony numbers was mild compared with *Setdb1*$^{\Delta/\Delta}$ LSK cells (supplemental Figure 2E).

We next transplanted BM cells from *Cre-ERT* control and *Cre-ERT;Setdb1*$^{fl/fl}$ mice with competitor cells into lethally irradiated WT recipient mice. After the deletion of *Setdb1*, the chimerism of *Setdb1*$^{\Delta/\Delta}$ hematopoietic cells significantly decreased in PB (Figure 1K), and *Setdb1*$^{\Delta/\Delta}$ LSK HSPCs in BM were completely depleted by 6 months (data not shown).

To test the role of *Setdb1* in cancer stem cells, we used a myeloid leukemia model induced by the leukemic fusion gene *MLL-AF9*.[18] We purified GMPs from *Cre-ERT* control and *Cre-ERT;Setdb1*$^{fl/fl}$ mice and transduced them with an *MLL-AF9* retrovirus (Figure 2A). We found that the proliferation of transformed GMPs was severely compromised after the deletion of *Setdb1* in liquid culture (Figure 2B) and in colony replating assays (Figure 2C). We then transplanted transformed GMPs into lethally irradiated recipient mice, along with wild-type BM cells for radioprotection. After confirming the development of overt leukemia, we injected tamoxifen from day 21 to delete *Setdb1*. Although the deletion of *Setdb1* significantly prolonged the survival of recipient mice, all mice eventually died (Figure 2D). Genomic PCR demonstrated the efficient deletion of *Setdb1* in leukemic cells immediately after the injection of tamoxifen. However, leukemic cells from moribund mice retained the floxed allele (Figure 2E), suggesting that only the leukemic cells that retained at least 1 floxed allele (escapers) gradually expanded and induced lethal leukemia. Moreover, *SETDB1* knockdown significantly suppressed the growth of human leukemic cells (HL-60 and K562 cells) (supplemental Figure 3). These results indicate that *Setdb1* also plays an essential role in leukemic stem cells.

### Setdb1 is mostly dispensable for the silencing of ERVs in HSPCs

To investigate the effects of the *Setdb1* deletion in HSPCs, we performed chromatin immunoprecipitation followed by the sequencing (ChIP-seq) of H3K9me3 and H3K9/K14 acetylation (ac) in WT and *Setdb1*$^{\Delta/\Delta}$ GMPs and RNA-sequencing (RNA-seq) of *Setdb1*$^{\Delta/\Delta}$ LSK cells and GMPs recovered from recipient mice 2 weeks after the deletion of *Setdb1*. Although western blot analysis did not reveal any significant difference in global H3K9me3 levels (supplemental Figure 4A), ChIP-seq detected changes in the levels of H3K9me3 between WT and *Setdb1*$^{\Delta/\Delta}$ GMPs (supplemental Figure 4B). Significant reductions were observed at ERV genome regions such as endogenous retrovirus-1 (ERV1) (class 1), intracisternal A-particle (IAP) (class 2), and endogenous retrovirus-like elements (class 3), and the promoters of coding genes (4.0 kb ± TSS). However, the reductions observed in H3K9me3 levels at ERV genome regions were milder than previously reported changes in ESCs[2,4] (supplemental Figure 4B). Furthermore, RRBS revealed that DNA methylation was maintained at high levels in *Setdb1*$^{\Delta/\Delta}$ LSK cells and GMPs (supplemental Figure 4C). Correspondingly, the deletion of *Setdb1* in HSPCs did not induce the high-level activation of ERVs (supplemental Figure 5). Although class 1 (ERV1) and class 2 (IAP and early transposon element), but not class 3 (mouse transposon A, murine endogenous retrovirus-L) and long interspersed elements, showed slight upregulation in a similar manner to *Setdb1*$^{\Delta/\Delta}$ ESCs, the levels of activation were very mild, particularly in LSK cells, compared with in *Setdb1*$^{\Delta/\Delta}$ ESCs, and fold upregulation was less than 2.0 on average, even in GMPs (supplemental Figure 5A). In *Setdb1*$^{\Delta/\Delta}$ ESCs and the developing brain, the activation of the long terminal repeat of ERVs, such as IAPs, has been shown to lead to the ectopic upregulation of neighboring genes, generating chimeric transcripts starting from ERVs.[4,5] A RNA-seq analysis revealed no chimeric transcripts for genes highly derepressed in *Setdb1*$^{\Delta/\Delta}$ LSK cells and GMPs listed in Figure 3, such as *Fbp1*, *Fbp2*, and epithelial cell adhesion molecule (Epcam), even though these gene loci have a number of neighboring and intronic ERV sequences (supplemental Figure 5B). Chimeric transcripts were not detected, even with the selected ERV loci showing significant derepression in *Setdb1*$^{\Delta/\Delta}$ LSK cells and GMPs (data not shown). These results indicate that the effect of Setdb1 loss on the silencing of ERVs is limited in adult HSPCs.



**Figure 1. Deletion of Setdb1 leads to rapid depletion of HSPCs in BM.** (A) Deletion of *Setdb1* in *Cre-ERT;Setdb1*$^{fl/fl}$ BM Lin$^-$c-Kit$^+$ hematopoietic progenitor cells were confirmed by genomic PCR 2 weeks after the first injection of tamoxifen. "WT," "floxed," and "Δ" alleles indicate the wild-type *Setdb1* allele, floxed *Setdb1* allele, and floxed *Setdb1* allele after the removal of exons 15 and 16 by Cre recombinase, respectively. (B) RT-PCR of *Setdb1* expression in LSK HSPCs 2 weeks after the first injection of tamoxifen. mRNA levels were normalized to *Hprt1* expression, and relative expression levels are shown as the mean ± SD of triplicate analyses. (C) Survival curve of recipient mice repopulated with BM cells from *Cre-ERT* (WT) and *Cre-ERT;Setdb1*$^{fl/fl}$ (*Setdb1*$^{\Delta/\Delta}$) mice after the initial injection of tamoxifen (n = 10). BM cells from 8-week-old *Cre-ERT* and *Cre-ERT;Setdb1*$^{fl/fl}$ mice were transplanted into lethally irradiated recipient mice without competitor cells. At 4 weeks after transplantation, recipient mice were injected with tamoxifen for 5 consecutive days. (D) Representative hematoxylin and eosin staining of BM sections from WT and moribund *Setdb1*$^{\Delta/\Delta}$ mice in (C). (E) The proportions of Mac-1$^+$ myeloid, B220$^+$ B, and CD4$^+$ or CD8$^+$ T cells among CD45.2$^+$ donor-derived hematopoietic cells in PB from WT and *Setdb1*$^{\Delta/\Delta}$ mice (n = 4) 2 weeks after the first injection of tamoxifen. Data are shown as the mean ± SD. (F) Absolute numbers of total BM cells, CD34$^-$LSK HSCs, CD34$^+$LSK multipotent progenitor cells, common myeloid progenitors, GMPs, and megakaryocyte/erythrocyte progenitors in the unilateral femur and tibia of WT and *Setdb1*$^{\Delta/\Delta}$ mice (n = 4) 2 weeks after the first injection of tamoxifen. Data are shown as the mean ± SD. (G) Percentage of Annexin V$^+$ cells in BM LSK and LK cells in WT (n = 4) and *Setdb1*$^{\Delta/\Delta}$ mice (n = 6) 9 days after the first injection of tamoxifen. Data are shown as the mean ± SD. (H) Representative flow cytometry profiles of the incorporation of Pyronin Y by BM CD45.2$^+$ LSK cells 2 weeks after the first injection of tamoxifen (left). The percentage of Pyronin Y$^+$ cells in LSK cells in WT and *Setdb1*$^{\Delta/\Delta}$ mice (n = 4) are shown as the mean ± SD (right). (I) Cell cycle status of LSK and Lin$^-$c-Kit$^+$ Sca-1$^-$ (LKS$^-$) committed progenitor cells evaluated by BrdU short-labeling assays. BrdU was administered 12 and 24 hours before the analysis to mark cells that entered S phase. Data are shown as the mean ± SD (n = 6). (J) Colony-forming assays with LSK cells from WT and *Setdb1*$^{\Delta/\Delta}$ mice 2 weeks after the initial injection of tamoxifen. The absolute numbers of colonies with the indicated size per 200 LSK cells are shown as the mean ± SD of triplicate cultures. (K) Competitive reconstitution assays. BM cells from 8-week-old *CreERT* and *CreERT;Setdb1*$^{fl/fl}$ mice ($2 \times 10^6$ cells) were transplanted into lethally irradiated recipient mice with competitor BM cells ($1 \times 10^6$ cells). At 8 weeks after transplantation, recipient mice were injected with tamoxifen for 5 consecutive days. The chimerism of CD45.2$^+$ donor-derived cells in all CD45$^+$ cells and in myeloid, B, and T cells in the PB of recipient mice is shown as the mean ± SD (n = 5). *$P < .05$; **$P < .01$; ***$P < .001$; ns, not significant.

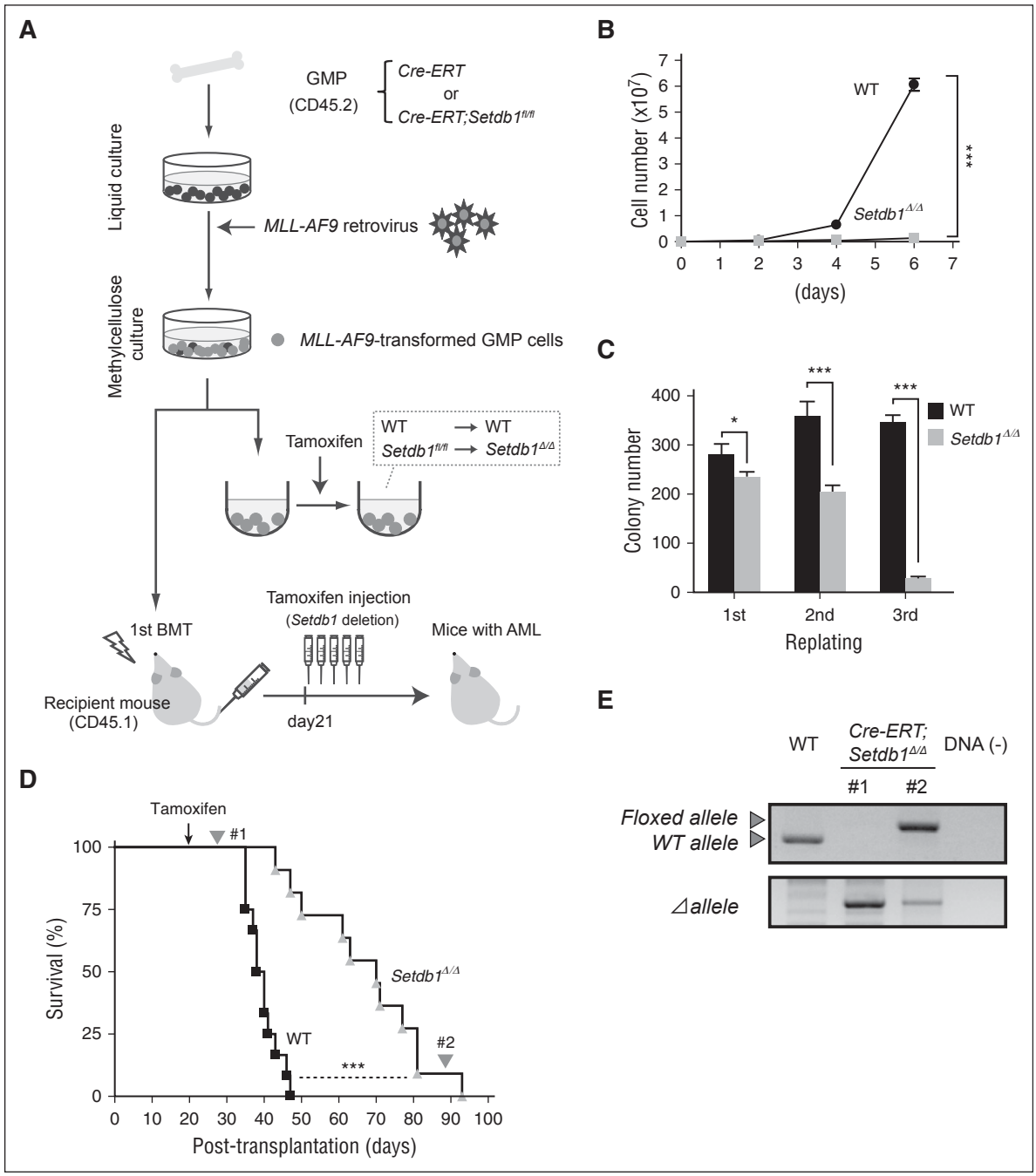


**Figure 2. Role of Setdb1 in leukemic stem cells.** (A) A schematic diagram of the experimental process. GMPs from *CreERT* and *CreERT;Setdb1$^{fl/fl}$* mice were transduced with *MLL-AF9* and cultured in methylcellulose medium. To delete *Setdb1* in vitro, *MLL-AF9*-transformed GMPs were transferred to liquid medium containing 200 nM 4-hydroxy tamoxifen (4-OHT). *MLL-AF9*-transformed GMPs were also transplanted into lethally irradiated recipient mice, together with WT BM cells for radioprotection. To delete *Setdb1* in vivo, tamoxifen was intraperitoneally injected once a day for 5 consecutive days at 21 days after transplantation. (B) Growth of *MLL-AF9*-transformed GMPs after the deletion of *Setdb1*. *MLL-AF9*-transformed GMPs ($1 \times 10^4$ cells each) were cultured in IMDM with 20% fetal calf serum, SCF, FP6, GM-CSF, and IL-3 (10 ng/mL each). Data are shown as the mean ± SD of triplicate cultures. (C) Replating efficiency of *MLL-AF9*-transformed GMPs after the deletion of *Setdb1*. *MLL-AF9*-transformed GMPs (1500 cells) were serially replated in methylcellulose medium containing 10 ng/mL SCF, 10 ng/mL FP6, 10 ng/mL GM-CSF, 10 ng/mL IL-3, and 100 nM 4-OHT. Data are shown as the mean ± SD of triplicate cultures. (D) Overall survival of mice injected with $4 \times 10^5$ WT or *Setdb1$^{\Delta/\Delta}$ MLL-AF9*-transformed cells compared by a Kaplan-Meier analysis (WT, n = 10; *Setdb1$^{\Delta/\Delta}$* n = 9). (E) The efficiency of the deletion of *Setdb1* in *MLL-AF9*-transformed GMPs was monitored. Genomic PCR data of leukemic cells immediately after the injection of tamoxifen and from moribund mice (#1 and #2, respectively, indicated in panel D). *$P < .05$; **$P < .01$; ***$P < .001$.

### Nonhematopoietic genes are ectopically activated in *Setdb1*-deficient HSPCs

We next analyzed changes in the expression of NCBI reference sequence (RefSeq) genes.[19] The genes derepressed (≥2-fold) in *Setdb1$^{\Delta/\Delta}$* LSK cells and GMPs included many nonhematopoietic genes (Figure 3A; supplemental Figure 5B), such as *Fbp2* and *Fbp1*, gluconeogenic enzyme genes specific to muscle and liver, respectively, and *Epcam*, an epithelial cell-specific cell surface glycoprotein that mediates $Ca^{2+}$-independent homophilic cell–cell adhesion and regulates cell migration.[20] A mega-analysis of the gene expression database using the online software tool ExAtlas[21] revealed that derepressed genes (≥2-fold) were

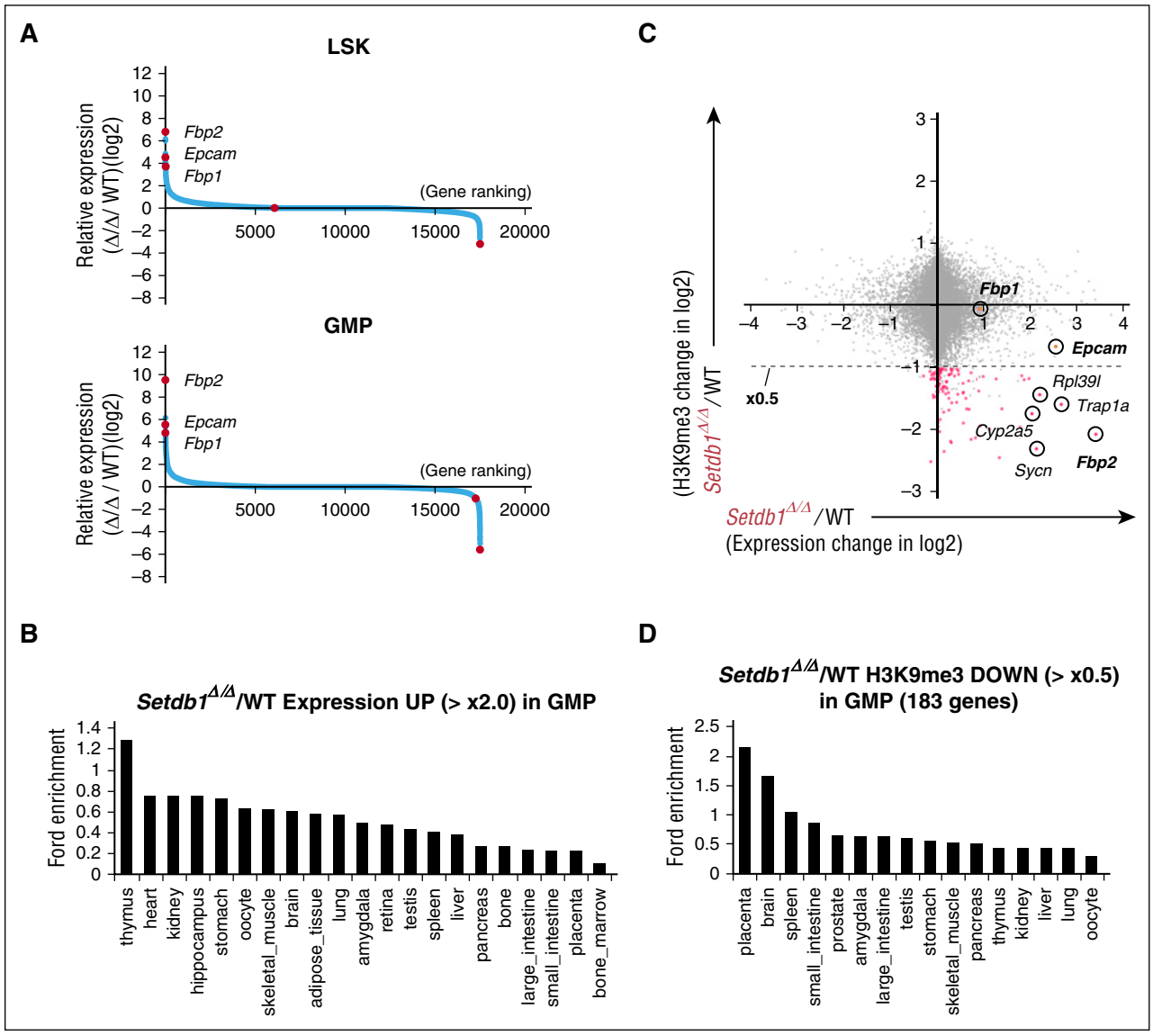


**Figure 3. Nonhematopoietic genes are ectopically activated in *Setdb1*-deficient HSPCs.** (A) Sequential plots of genes according to fold expression changes in *Setdb1*$^{\Delta/\Delta}$ LSK cells and GMPs from WT cells 2 weeks after the first injection of tamoxifen detected by RNA-seq. Representative genes with significant expression changes are indicated. (B) Enrichment of organ-specific genes in upregulated genes (≥×2.0) in *Setdb1*$^{\Delta/\Delta}$ GMPs. The enrichment of genes preferentially expressed in each organ and tissue in the above gene set was calculated by ExAtlas software (http://lgsun.grc.nia.nih.gov/exatlas/). (C) A scatter plot showing the correlation between H3K9me3 levels and the expression levels of RefSeq genes in *Setdb1*$^{\Delta/\Delta}$ GMPs relative to WT GMPs. The 183 genes showing reductions in H3K9me3 levels greater than 2-fold (below dotted line) are indicated in red dots. (D) Enrichment of organ-specific genes in 183 genes losing H3K9me3 greater than 2-fold in *Setdb1*$^{\Delta/\Delta}$ GMPs among genes that showed H3K9me3 enrichment greater than 2-fold over the input signal in (C). The enrichment of genes preferentially expressed in each organ and tissue in the above gene set was calculated by ExAtlas software, as in (B).

largely nonhematopoietic genes (Figure 3B). We compared ChIP-seq data for H3K9me3 levels with RNA-seq data in GMPs. Among the genes that showed H3K9me3 enrichment greater than 2-fold over the input signal at promoters (4.0 kb ± TSS), 183 genes (indicated in red dots in Figure 3C) reduced H3K9me3 levels by more than 2-fold in *Setdb1*$^{\Delta/\Delta}$ GMPs than in WT. These genes were assumed to be potential direct targets of Setdb1, showed a trend toward upregulation in expression levels (Figure 3C), and were also enriched for nonhematopoietic genes in the mega-analysis (Figure 3D).

Among these genes, *Fbp2*, but not *Fbp1*, showed a clear reduction in H3K9me3 levels at the promoter (Figure 4A) and DNA methylation levels around the TSS and in the gene body in *Setdb1*$^{\Delta/\Delta}$ GMPs (Figure 4B). Reductions in H3K9me3 levels were also confirmed in *Setdb1*$^{\Delta/\Delta}$ LSK cells and GMPs by manual ChIP assays (Figure 4C). In contrast, H3K9/14ac levels were increased in the absence of Setdb1 (Figures 4A,C). Although the *Epcam* promoter was marked with H3K9me3 at a low level, H3K9me3 was completely lost in *Setdb1*$^{\Delta/\Delta}$ GMPs (Figure 4A). These results suggest that *Fbp2* and *Epcam* are direct targets of Setdb1.

To directly analyze the expression profile of HSCs, we performed single-cell expression profiling, using the Fluidigm system, because of the limited number of available *Setdb1*$^{\Delta/\Delta}$ HSCs. The expression of representative HSC genes was maintained well in *Setdb1*$^{\Delta/\Delta}$ CD34$^{-}$ LSK HSCs (supplemental Figure 6). As in LSK cells and GMPs, however, *Epcam* was derepressed at high levels in HSCs, whereas *Fbp2* was not (supplemental Figure 6). A flow cytometric analysis readily detected the upregulation of Epcam in *Setdb1*$^{\Delta/\Delta}$ LSK cells and GMPs (Figure 4D).

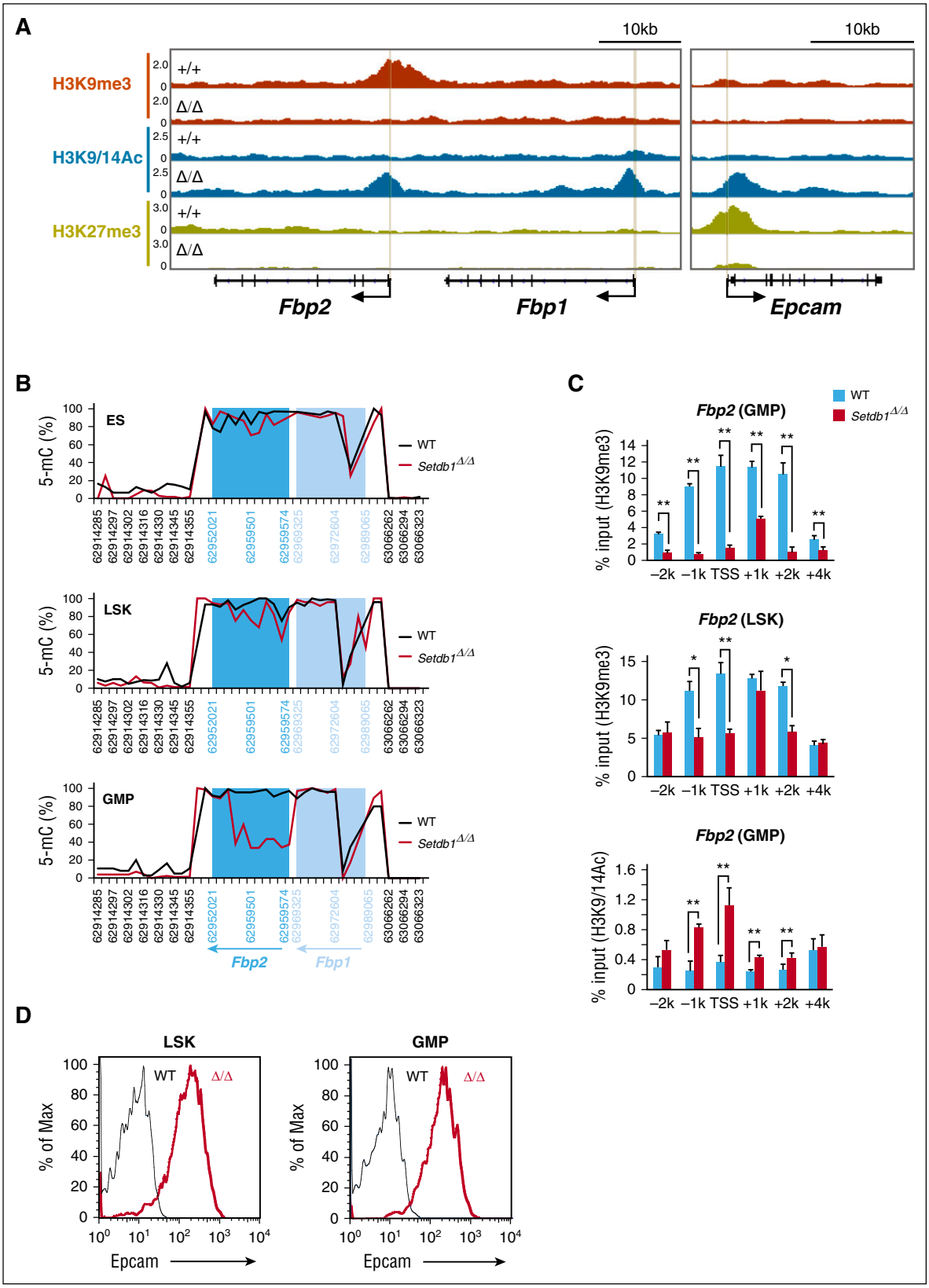


**Figure 4. Derepression of gluconeogenic genes and *Epcam* in *Setdb1*-deficient HSPCs.** (A) Visualization of ChIP-sequence data of the levels of H3K9me3, H3K9/14ac, and H3K27me3 at the *Fbp2*, *Fbp1*, and *Epcam* gene loci in WT and *Setdb1*$^{\Delta/\Delta}$ GMPs, using the Integrative Genomics Viewer. Schematic diagrams of these gene loci indicate their genomic structures. Exons and untranslated regions are demarcated by large and small black boxes, respectively. (B) DNA methylation status at the *Fbp2* and *Fbp1* gene loci detected by RRBS in WT and *Setdb1*$^{\Delta/\Delta}$ ESCs and LSK cells and GMPs from WT and *Setdb1*$^{\Delta/\Delta}$ mice. The proportions of methylated cytosine are depicted. (C) Manual ChIP assays for H3K9me3 and H3K9/14Ac at the *Fbp2* loci using anti-H3K9me3 and H3K9/14Ac antibodies. The relative amounts of immunoprecipitated DNA are depicted as a percentage of input DNA. Data are shown as the mean ± SD (n = 3). (D) Flow cytometric profiles of BM *Setdb1*$^{\Delta/\Delta}$ LSK cells and GMPs 2 weeks after the first injection of tamoxifen for Epcam expression.

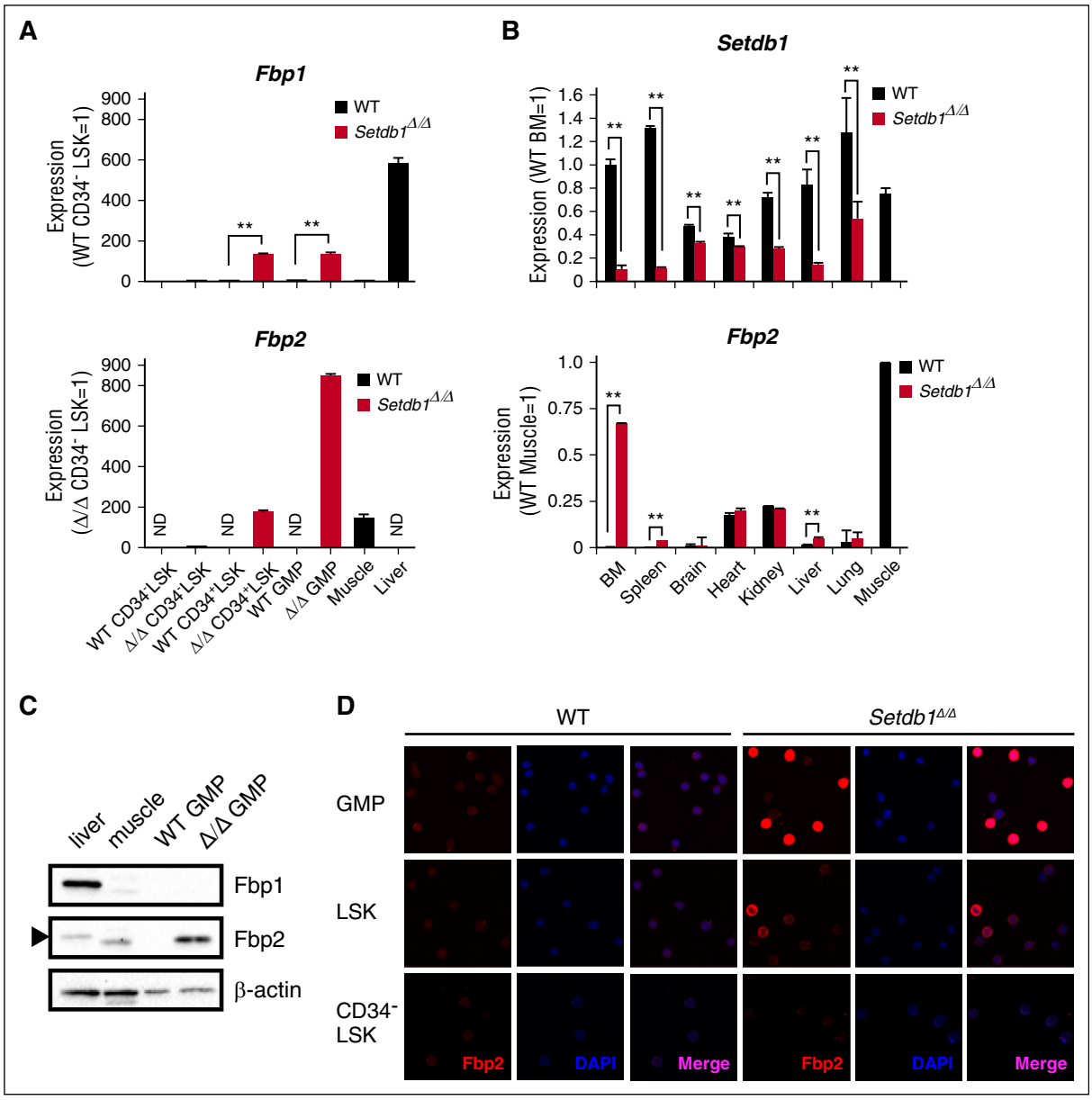


**Figure 5. Ectopic activation of Fbp2 in *Setdb1*-deficient HSPCs.** (A) RT-PCR of *Fbp1* and *Fbp2* expression in the indicated cells from WT mice. mRNA levels were normalized to *Hprt1* expression, and relative expression levels are shown as the mean ± SD of triplicate analyses. ND, not detected. $^{**}P < .01$. (B) RT-PCR of *Setdb1* and *Fbp2* expression in the indicated organs from WT and *Setdb1*$^{\Delta/\Delta}$ mice 7 days after the first injection of tamoxifen. mRNA levels were normalized to *Hprt1* expression, and relative expression levels are shown as the mean ± SD of triplicate analyses. $^{**}P < .01$. (C) A western blot analysis of Fbp1 and Fbp2 protein expression in GMPs from WT and *Setdb1*$^{\Delta/\Delta}$ mice 2 weeks after the first injection of tamoxifen. Liver and muscle were used as references, and β-actin was probed as a loading control. The arrowhead indicates a cross-reactive Fbp1 signal in lane 1. (D) Immunostaining of Fbp2 in CD34$^{-}$LSK HSCs, LSK HSPCs, and GMPs from WT and *Setdb1*$^{\Delta/\Delta}$ mice 2 weeks after the first injection of tamoxifen. Cells were counterstained with DAPI. Representative images are depicted.

### Metabolic homeostasis is impaired in *Setdb1*-deficient HSPCs

Fbp1 and Fbp2 are enzymes that convert fructose-1,6-bisphosphate (F-1,6-BP) to fructose 6-phosphate (F6P) in gluconeogenesis and counteract the reaction catalyzed by phosphofructokinase (Pfk) in glycolysis (supplemental Figure 8).[22] Although the *Fbp1* and *Fbp2* loci are in very close proximity (Figure 4A), they are differentially expressed in the gluconeogenic tissues (the liver and kidney and the muscle, respectively) (Figure 5A). In the absence of Setdb1, *Fbp2* was highly derepressed in *Setdb1*$^{\Delta/\Delta}$ CD34$^{+}$LSK cells and GMPs at levels similar to and greater than those in muscle, respectively (Figure 5A). Fbp2 protein was readily detected in *Setdb1*$^{\Delta/\Delta}$ GMPs by a western blot analysis (Figure 5C), and in *Setdb1*$^{\Delta/\Delta}$ LSK cells and GMPs but not CD34$^{-}$LSK HSCs by an immunofluorescence staining (Figure 5D). *Fbp2* appeared to be activated specifically in BM cells among major organs upon the deletion of *Setdb1* (Figure 5B). *Fbp1* was also derepressed in *Setdb1*$^{\Delta/\Delta}$ LSK cells and GMPs to a quarter of the level in the liver (Figure 5A). However, Fbp1 protein was not detected in *Setdb1*$^{\Delta/\Delta}$ GMPs (Figure 5C). These results indicate that both *Fbp1* and *Fbp2* were ectopically activated in *Setdb1*$^{\Delta/\Delta}$ HSPCs, but only Fbp2 was overexpressed at the protein level. Of interest, *Fbp1* and *Fbp2* were both maintained in a transcriptionally repressed

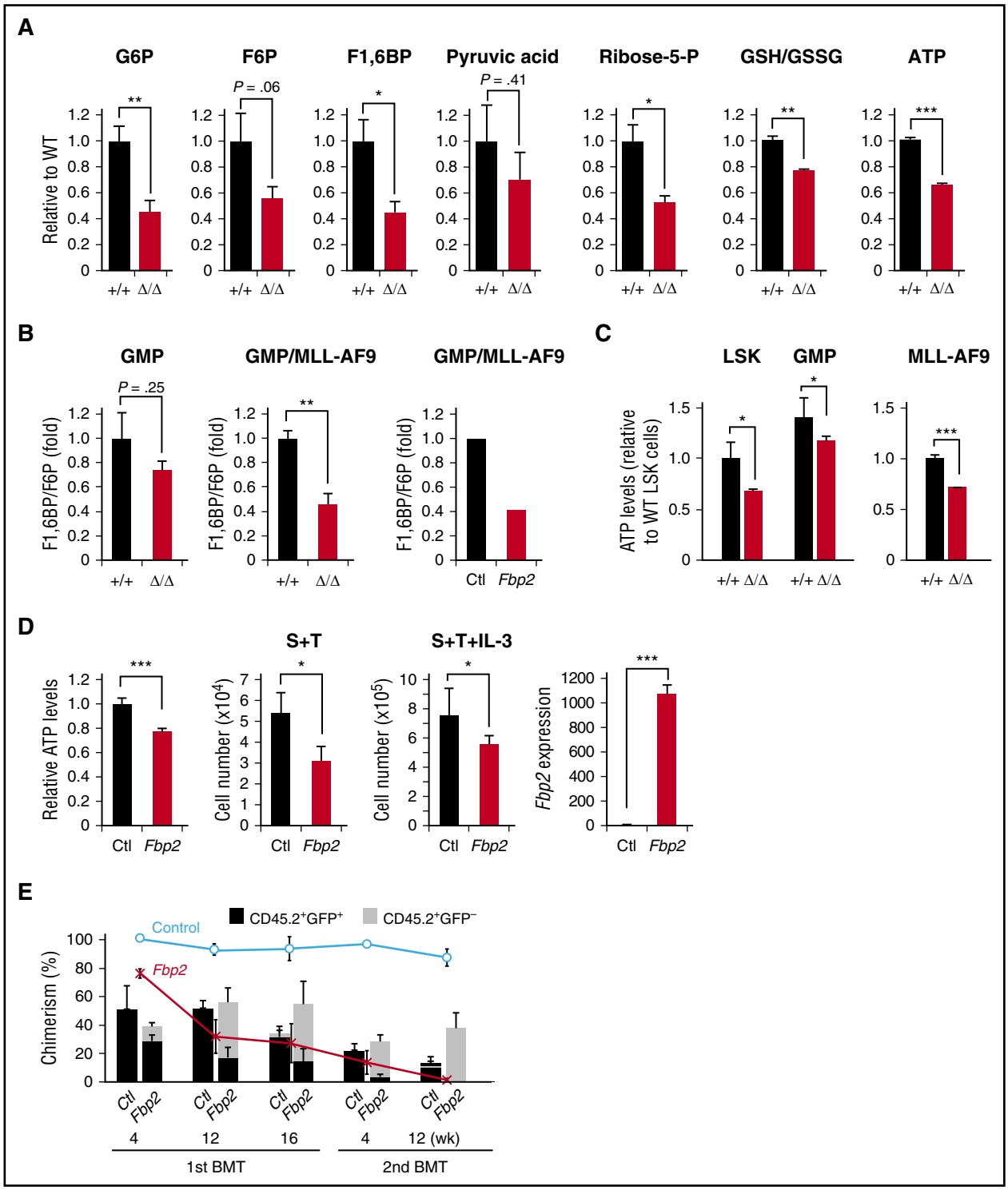


**Figure 6. Metabolic homeostasis is impaired in *Setdb1*-deficient HSPCs.** (A) Results of metabolome analyses of GMPs freshly isolated from *Setdb1*$^{\Delta/\Delta}$ mice 2 weeks after the first injection of tamoxifen. Relative values (WT values were set as 1) are shown as the mean ± SD (glucose 6-phosphate, F6P, F1,6BP, n = 4-6; pyruvic acid, n = 2; ribose-5-P, reduced glutathione/oxidized glutathione, n = 3; ATP, n = 9). (B) F1,6BP levels relative to F6P in GMPs (n = 4), *MLL-AF9*-transformed GMPs 48 hours after the tamoxifen treatment (n = 3), and *MLL-AF9*-transformed GMPs overexpressing *Fbp2* (n = 1). (C) ATP levels in LSK cells and GMPs freshly isolated from *Setdb1*$^{\Delta/\Delta}$ mice 2 weeks after the first injection of tamoxifen and *MLL-AF9*-transformed GMPs 48 hours after the tamoxifen treatment. Data are shown as the mean ± SD (n = 3). (D) ATP levels in LSK cells transduced with an *Fbp2* retrovirus in culture (left) and their growth in culture supplemented with SCF (10 ng/mL) and thrombopoietin (10 ng/mL) without or with IL-3 (10 ng/mL). mRNA levels of exogenous *Setdb1* in LSK cells detected by RT-PCR were normalized to *Hprt1* expression. (Right) Relative expression levels. Data are shown as the mean ± SD (n = 3). (E) Repopulating capacity of *Fbp2*-overexpressing HSCs in vivo. Fifty CD45.2 CD34$^-$LSK HSCs were transduced either with a control or *Fbp2* retrovirus, and then transplanted into lethally irradiated CD45.1 mice (n = 6) with 2 × 10$^5$ CD45.1 competitor cells. The chimerism of CD45.2$^+$GFP$^+$ cells derived from transduced HSCs as well as CD45.2$^+$GFP$^-$ cells derived from nontransduced HSCs was monitored. At 16 weeks after primary transplantation, all BM cells from recipients were pooled and 1 × 10$^7$ cells were infused into the secondary recipients. The proportions of GFP$^+$ cells in donor-derived cells are plotted in blue (control) and red (*Fbp2*) lines. **P* < .05; ***P* < .01; ****P* < .001.

state in *Setdb1*$^{\Delta/\Delta}$ CD34$^{-}$LSK HSCs (Figure 5A; supplemental Figure 6).

Fbp1 and Fbp2 are the rate-limiting enzymes of gluconeogenesis. Fbp1 has recently been identified as a critical regulator of glucose metabolism in renal cell carcinoma.[23] To elucidate the effect of the ectopic expression of Fbp2 in hematopoietic progenitor cells, we performed a metabolome analysis. The metabolites at the early steps of glycolysis, including glucose 6-phosphate, F6P, and F-1,6-BP, were all decreased in freshly isolated *Setdb1*$^{\Delta/\Delta}$ GMPs (Figure 6A; supplemental Figure 8). In contrast, pyruvic acid, a downstream metabolite, showed a mild reduction. Notably, F-1,6-BP levels relative to F6P levels (F-1,6-BP/F6P) were lower in *Setdb1*$^{\Delta/\Delta}$ GMPs and *Setdb1*$^{\Delta/\Delta}$ *MLL-AF9*-transformed GMPs, as well as in *MLL-AF9*-transformed GMPs overexpressing *Fbp2* (Figure 6B), suggesting Fbp2 antagonizes the glycolytic flux in hematopoietic progenitor cells. In addition, the levels of ribose 5-phosphate (ribose 5-P), which is used in the synthesis of nucleotides and nucleic acids, and the ratio of reduced glutathione to oxidized glutathione (reduced glutathione/oxidized glutathione) were decreased in *Setdb1*$^{\Delta/\Delta}$ GMPs (Figure 6A; supplemental Figure 8). Given the reduction in glucose 6-phosphate levels, the entry metabolite of the pentose phosphate pathway, Fbp2 also affects the pentose phosphate pathway flux by regulating glycolysis similar to Fbp1 in renal cell carcinoma (supplemental Figure 8).[23] We then investigated the consequence of compromised metabolism in *Setdb1*$^{\Delta/\Delta}$ HSPCs. ATP levels were significantly reduced not only in GMPs (Figure 6A,C) but also in LSK cells and *MLL-AF9*-transformed GMPs in the absence of Setdb1 (Figure 6C).

The ectopic overexpression of *Fbp2* in HSPCs significantly reduced their ATP levels and significantly inhibited the cell growth of primitive HSPCs in liquid culture supplemented with stem cell factor (SCF) and thrombopoietin (S+T), as well as in that supplemented with multiple cytokines containing interleukin 3 (IL-3) (S+T+IL-3) (Figure 6D). In competitive repopulating assays, the repopulating capacity of CD45.2$^{+}$ GFP$^{+}$ HSPCs overexpressing *Fbp2* was also found to be impaired, and these cells were eventually depleted in the secondary recipient mice (Figure 6E).

We attempted rescue experiments of *Setdb1*$^{\Delta/\Delta}$ *MLL-AF9*-transformed GMPs by exogenous Setdb1. We infected cells with retroviruses harboring either full-length *Setdb1* or short-form *Setdb1* truncated for the portion encoding the SET catalytic domain (*ΔSET*) and then deleted endogenous *Setdb1* by adding tamoxifen in culture (supplemental Figure 7A,B). Full-length *Setdb1* largely restored the proliferative capacity of *Setdb1*$^{\Delta/\Delta}$ cells and maintained the transcriptional repression of *Fbp2* and ATP levels. In contrast, the effects of *ΔSET* were minimal, suggesting the requirement of the enzymatic activity of *Setdb1* in gene silencing and maintenance of HSPCs. We further tested knockdown of *Fpb2* and overexpression of *Pfk1* in *Setdb1*$^{\Delta/\Delta}$ *MLL-AF9*-transformed GMPs. Both partially but significantly restored ATP levels. However, impaired cell growth was not rescued at all (supplemental Figure 7C,D).

## Discussion

The histone methyltransferases responsible for H3K9me3, such as Suv39h and Setdb1, play key roles in the gene silencing of retroelements, including long interspersed elements and ERVs in cells of embryonic origin. In contrast, DNA methylation is mainly responsible for silencing in differentiated cells such as neural progenitor cells and fibroblasts, whereas histone methyltransferases are largely dispensable.[2,24] Setdb1 was recently shown to contribute to the silencing of ERVs in B lymphocytes; however, the transcriptional activation of ERVs was dependent on the regulatory architecture of their long terminal repeats and the availability of corresponding B-cell-specific transcription factors such as Pax5.[25] In the present study, we found that H3K9me3 and DNA methylation were not largely altered at ERV loci and derepression of ERVs was minimal in the absence of Setdb1. These results confirm previous findings obtained in neural progenitor cells and fibroblasts[2,24] and highlight the important role of DNA methylation in the silencing of ERVs in HSPCs.

In the present study, we clearly demonstrated that Setdb1 is the first H3K9 histone methyltransferase to be identified as an essential regulator of HSPCs. G9a/GLP, which catalyzes H3K9me2, has been shown to promote progressive H3K9me2 patterning during HSPC lineage specification, and its inhibition delays HSPC lineage commitment.[7,26] G9a is dispensable for HSPCs, but plays a critical role in the proliferation of acute myeloid leukemia by regulating HoxA9-dependent transcription.[8] Thus, the role of Setdb1 in HSPCs is in marked contrast to that of G9a and corresponds to that of Kap1, a binding partner of Setdb1.[9] In the absence of Setdb1, we found only a limited number of genes losing H3K9me3 levels in hematopoietic progenitors, which appeared to be mostly nonhematopoietic genes. However, not all of them became activated, which may have been a result of the absence of transcriptional factors compatible to their transcriptional regulatory architecture. It is also possible that the effects of Setdb1 loss on epigenome and transcription we observed in this study could be secondary to events resulting in loss of hematopoietic cells, rather than direct effects of Setdb1 loss. Nevertheless, among candidate Setdb1 target genes, a key gluconeogenic enzyme gene *Fbp2* was strongly activated in both HSPCs and *MLL-AF9*-transformed GMPs, suggesting that derepression of *Fbp2* is a direct effect of Setdb1 loss.

Gluconeogenesis occurs in a limited number of organs such as the liver, kidney, and muscle. Other organs, including HSPCs as well as cancer cells, favor glycolysis over the oxidative phosphorylation of glucose, and thus maintain *Fbp1* and *Fbp2*, in a transcriptionally repressed state.[27] *FBP1* and *FBP2* are strongly repressed, particularly in cancer cells, via mechanisms including the DNA hypermethylation of their promoters.[23,28,29] FBP1 and FBP2 both antagonize glycolysis in cancer cells, thereby inhibiting the Warburg effect. In contrast, the loss of FBP1 or FBP2 in cancer cells enhances glycolysis, resulting in the maintenance of ATP production and proliferative capacity under hypoxic conditions.[23,28,29] However, the regulation of gluconeogenic enzyme genes in HSPCs has not yet been characterized. In the present study, we showed that Setdb1-dependent H3K9me3, in concert with DNA methylation, targets *Fbp1* and *Fbp2*. Because the *Fbp2* promoter was marked with higher levels of H3K9me3 than the *Fbp1* promoter, *Fbp2* may be more dependent on Setdb1-dependent H3K9me3 for silencing, and the activation of Fbp1 could be an indirect event. Nevertheless, both *Fbp1* and *Fbp2* were maintained in a repressed state in CD34$^{-}$LSK HSCs, even in the absence of Setdb1, suggesting that *Fbp1* and *Fbp2* are more dependent on DNA methylation for silencing in HSCs.

The consequence of the ectopic expression of Fbp2 protein in HSPCs was very similar to that in cancer cells (supplemental Figure 8). It antagonized glycolysis and attenuated the production of ATP, resulting in an impaired repopulating capacity in HSPCs.

Fbp2 also affected the pentose phosphate pathway flux by antagonizing glycolysis similar to Fbp1.[23] Therefore, *Fbp2* is detrimental to HSPCs once activated, and has to be strongly repressed to maintain precise energy metabolism in HSPCs. Knockdown of *Fpb2* and overexpression of *Pfk1* in *Setdb1*$^{\Delta/\Delta}$ *MLL-AF9*-transformed GMPs partially but significantly restored ATP levels. Nonetheless, impaired cell growth was not rescued at all. These results support the notion that ectopic expression of *Fbp2* compromises energy production via glycolysis in HSPCs, while at the same time strongly suggesting that gluconeogenesis pathway is not the only causative pathway compromised in the absence of Setdb1.

Although *Fbp2* was maintained in a repressed state in *Setdb1*$^{\Delta/\Delta}$ HSCs, HSCs were depleted in a manner similar to HSPCs, suggesting that Setdb1 regulates multiple important targets in HSPCs. Although we could not directly evaluate apoptosis of HSCs because of the limited number of *Setdb1*$^{\Delta/\Delta}$ HSCs, we found that mitochondrial reactive oxygen species levels were significantly higher in *Setdb1*$^{\Delta/\Delta}$ HSCs. Together with the ectopic expression of Epcam in *Setdb1*$^{\Delta/\Delta}$ HSCs, multiple defects may be responsible for depletion of *Setdb1*$^{\Delta/\Delta}$ HSCs.

Although the epigenetic regulation of HSPCs has been extensively characterized, more information is needed. Together with our previous findings on *Kap1*-deficient HSPCs, the results of the present study clearly demonstrate that nonhematopoietic genes are permanently repressed in HSPCs via H3K9me-mediated silencing machineries in collaboration with DNA methylation. This silencing manner is in marked contrast to the transient as well as reversible silencing mediated by the polycomb-group complexes that maintain the multipotency of HSPCs.[30] The precise mechanisms by which these differential-silencing processes occur requires further study.

## Acknowledgments

The authors thank George R. Wendt for technical assistance and Ola Mohammed Kamel Rizq for critical review of the manuscript.

This work was supported in part by grants-in-aid for Scientific Research (#15639313) and Scientific Research on Innovative Areas "Stem Cell Aging and Disease" (#26115002) and "Genome Science" (#221S0002) from the Ministry of Education, Culture, Sports, Science and Technology (MEXT), Japan, Grant-in-Aid for Core Research for Evolutional Science and Technology from the Japan Science and Technology Corporation, and grants from the Uehara Foundation and Yasuda Foundation. S.K. is a research fellow supported by Japan Society for the Promotion of Science, MEXT, Japan.

## Authorship

Contribution: S.K. and A.I. designed this study; S.K. performed experiments, analyzed data, and actively wrote the manuscript; M.O., K.T., S.Y., E.N., A.S., K.A., Y.K., S.M., Y.N.-T., H.M., F.A., and Y.S. performed experiments and analyzed data; T.C., H.N., and T.S. provided analysis tools and analyzed data; H.K. provided antibodies; S.Y. provided mice; and A.I. conceived of and directed the project, secured funding, and actively wrote the manuscript.

Conflict-of-interest disclosure: The authors declare no competing financial interests.

Correspondence: Atsushi Iwama, Department of Cellular and Molecular Medicine, Graduate School of Medicine, Chiba University, 1-8-1 Inohana, Chuo-ku, Chiba 260-8670, Japan; e-mail: aiwama@faculty.chiba-u.jp.

## References

1. Du J, Johnson LM, Jacobsen SE, Patel DJ. DNA methylation pathways and their crosstalk with histone methylation. *Nat Rev Mol Cell Biol.* 2015; 16(9):519-532.
2. Matsui T, Leung D, Miyashita H, et al. Proviral silencing in embryonic stem cells requires the histone methyltransferase ESET. *Nature.* 2010; 464(7290):927-931.
3. Dodge JE, Kang YK, Beppu H, Lei H, Li E. Histone H3-K9 methyltransferase ESET is essential for early development. *Mol Cell Biol.* 2004;24(6): 2478-2486.
4. Karimi MM, Goyal P, Maksakova IA, et al. DNA methylation and SETDB1/H3K9me3 regulate predominantly distinct sets of genes, retroelements, and chimeric transcripts in mESCs. *Cell Stem Cell.* 2011;8(6):676-687.
5. Tan SL, Nishi M, Ohtsuka T, et al. Essential roles of the histone methyltransferase ESET in the epigenetic control of neural progenitor cells during development. *Development.* 2012;139(20): 3806-3816.
6. Rowe HM, Jakobsson J, Mesnard D, et al. KAP1 controls endogenous retroviruses in embryonic stem cells. *Nature.* 2010;463(7278):237-240.
7. Ugarte F, Sousae R, Cinquin B, et al. Progressive Chromatin Condensation and H3K9 Methylation Regulate the Differentiation of Embryonic and Hematopoietic Stem Cells. *Stem Cell Rep.* 2015; 5(5):728-740.
8. Lehnertz B, Pabst C, Su L, et al. The methyltransferase G9a regulates HoxA9-dependent transcription in AML. *Genes Dev.* 2014;28(4): 317-327.
9. Miyagi S, Koide S, Saraya A, et al. The TIF1β-HP1 system maintains transcriptional integrity of hematopoietic stem cells. *Stem Cell Rep.* 2014; 2(2):145-152.
10. Ohashi Y, Hirayama A, Ishikawa T, et al. Depiction of metabolome changes in histidine-starved Escherichia coli by CE-TOFMS. *Mol Biosyst.* 2008;4(2):135-147.
11. Ooga T, Sato H, Nagashima A, et al. Metabolomic anatomy of an animal model revealing homeostatic imbalances in dyslipidaemia. *Mol Biosyst.* 2011;7(4):1217-1223.
12. Sugimoto M, Wong DT, Hirayama A, Soga T, Tomita M. Capillary electrophoresis mass spectrometry-based saliva metabolomics identified oral, breast and pancreatic cancer-specific profiles. *Metabolomics.* 2010;6(1): 78-95.
13. Junker BH, Klukas C, Schreiber F. VANTED: a system for advanced data analysis and visualization in the context of biological networks. *BMC Bioinformatics.* 2006;7:109.
14. Day DS, Luquette LJ, Park PJ, Kharchenko PV. Estimating enrichment of repetitive elements from high-throughput sequence data. *Genome Biol.* 2010;11(6):R69.
15. Muto T, Sashida G, Oshima M, et al. Concurrent loss of *Ezh2* and *Tet2* cooperates in the pathogenesis of myelodysplastic disorders. *J Exp Med.* 2013;210(12):2627-2639.
16. Hayashi-Takanaka Y, Yamagata K, Wakayama T, et al. Tracking epigenetic histone modifications in single cells using Fab-based live endogenous modification labeling. *Nucleic Acids Res.* 2011; 39(15):6475-6488.
17. Akalin A, Kormaksson M, Li S, et al. methylKit: a comprehensive R package for the analysis of genome-wide DNA methylation profiles. *Genome Biol.* 2012;13(10):R87.
18. Krivtsov AV, Twomey D, Feng Z, et al. Transformation from committed progenitor to leukaemia stem cell initiated by MLL-AF9. *Nature.* 2006;442(7104):818-822.
19. Pruitt KD, Brown GR, Hiatt SM, et al. RefSeq: an update on mammalian reference sequences. *Nucleic Acids Res.* 2014;42(Database issue): D756-D763.
20. Schnell U, Cirulli V, Giepmans BN. EpCAM: structure and function in health and disease. *Biochim Biophys Acta.* 2013;1828(8): 1989-2001.
21. Sharov AA, Schlessinger D, Ko MS. ExAtlas: An interactive online tool for meta-analysis of gene expression data. *J Bioinform Comput Biol.* 2015; 13(6):1550019.
22. Dzugaj A. Localization and regulation of muscle fructose-1,6-bisphosphatase, the key enzyme of glyconeogenesis. *Adv Enzyme Regul.* 2006;46: 51-71. Epub2006Jul18.
23. Li B, Qiu B, Lee DS, et al. Fructose-1,6-bisphosphatase opposes renal carcinoma progression. *Nature.* 2014;513(7517): 251-255.
24. Bulut-Karslioglu A, De La Rosa-Velázquez IA, Ramirez F, et al. Suv39h-dependent H3K9me3 marks intact retrotransposons and silences LINE

elements in mouse embryonic stem cells. *Mol Cell.* 2014;55(2):277-290.

25. Collins PL, Kyle KE, Egawa T, Shinkai Y, Oltz EM. The histone methyltransferase SETDB1 represses endogenous and exogenous retroviruses in B lymphocytes. *Proc Natl Acad Sci USA.* 2015;112(27):8367-8372.
26. Chen X, Skutt-Kakaria K, Davison J, et al. G9a/GLP-dependent histone H3K9me2 patterning during human hematopoietic stem cell lineage commitment. *Genes Dev.* 2012;26(22):2499-2511.
27. Ito K, Suda T. Metabolic requirements for the maintenance of self-renewing stem cells. *Nat Rev Mol Cell Biol.* 2014;15(4):243-256.
28. Dong C, Yuan T, Wu Y, et al. Loss of FBP1 by Snail-mediated repression provides metabolic advantages in basal-like breast cancer. *Cancer Cell.* 2013;23(3):316-331.
29. Li H, Wang J, Xu H, et al. Decreased fructose-1,6-bisphosphatase-2 expression promotes glycolysis and growth in gastric cancer cells. *Mol Cancer.* 2013;12(1):110.
30. Oshima M, Iwama A. Epigenetics of hematopoietic stem cell aging and disease. *Int J Hematol.* 2014;100(4):326-334.